

Diffuse optical assessment of cerebral-autoregulation in older adults stratified by cerebrovascular risk

Ahmed A. Bahrani^{1,2,3}  | Weikai Kong¹ | Yu Shang⁴ | Chong Huang¹ | Charles D. Smith^{2,5,6} | David K. Powell^{5,7} | Yang Jiang^{2,5,8} | Abner O. Rayapati⁹ | Gregory A. Jicha^{2,5,6} | Guoqiang Yu^{1*}

¹Department of Biomedical Engineering, University of Kentucky, Lexington, Kentucky

²Sanders-Brown Center on Aging, University of Kentucky, Lexington, Kentucky

³Biomedical Engineering Department, Al-Khwarizmi College of Engineering, University of Baghdad, Baghdad, Iraq

⁴Shanxi Provincial Key Laboratory for Biomedical Imaging and Big Data, North University of China, Shanxi, China

⁵Magnetic Resonance Imaging and Spectroscopy Center (MRISC), University of Kentucky, Lexington, Kentucky

⁶Department of Neurology, University of Kentucky, Lexington, Kentucky

⁷Neuroscience Department, University of Kentucky, Lexington, Kentucky

⁸Department of Behavioral Science, University of Kentucky, Lexington, Kentucky

⁹Department of Psychiatry, University of Kentucky, Lexington, Kentucky

*Correspondence

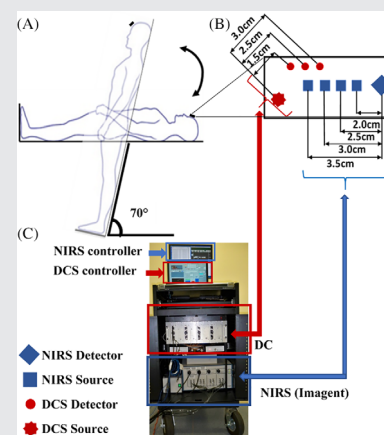
Guoqiang Yu, Department of Biomedical Engineering, University of Kentucky, Lexington, KY 40506.
Email: guoqiang.yu@uky.edu

Funding information

American Heart Association, Grant/Award Number: 16GIA30820006; Higher Committee for Education Development in Iraq, Grant/Award Number: Supporting the primary author scholarship; National Institutes of Health, Grant/Award Numbers: 1R01AG062480, 5P30AG028383, R01-HD101508, R21-HD091118; National Science Foundation (NSF), Grant/Award Number: EPSCoR1539068

Abstract

Diagnosis of cerebrovascular disease (CVD) at early stages is essential for preventing sequential complications. CVD is often associated with abnormal cerebral microvasculature, which may impact cerebral-autoregulation (CA). A novel hybrid near-infrared diffuse optical instrument and a finger plethysmograph were used to simultaneously detect low-frequency oscillations (LFOs) of cerebral blood flow (CBF), oxy-hemoglobin concentration ([HbO₂]), deoxy-hemoglobin concentration ([Hb]) and mean arterial pressure (MAP) in older adults before, during and after 70° head-up-tilting (HUT). The participants with valid data were divided based on Framingham risk score (FRS, 1-30 points) into low-risk (FRS ≤15, n = 13) and high-risk (FRS >15, n = 11) groups for developing CVD. The LFO gains were determined by transfer function analyses with MAP as the input, and CBF, [HbO₂] and [Hb] as the outputs ($CA \propto 1/\text{Gain}$). At resting-baseline, LFO gains



Abbreviations: [Hb], deoxy-hemoglobin concentration; [HbO₂], oxy-hemoglobin concentration; CA, cerebral-autoregulation; CBF, cerebral blood flow; CSD, cross-spectral density; CVD, cerebrovascular disease; DCS, diffuse correlation spectroscopy; FFT, fast Fourier transform; FRS, Framingham risk score; HUT, head-up-tilting; LFO, low-frequency oscillation; MAP, mean arterial pressure; NIRS, near-infrared spectroscopy; PSD, power spectral density; S-D, source-detector; SNR, signal-to-noise ratio.

in the high-risk group were relatively lower compared to the low-risk group. The lower baseline gains in the high-risk group may attribute to compensatory mechanisms to maintain stronger steady-state CAs. However, HUT resulted in smaller gain reductions in the high-risk group compared to the low-risk group, suggesting weaker dynamic CAs. LFO gains are potentially valuable biomarkers for early detection of CVD based on associations with CAs.

KEYWORDS

cerebral blood flow, cerebral blood oxygenation, cerebral-autoregulation, cerebrovascular disease, diffuse correlation spectroscopy, head-up-tilting, low-frequency oscillation, near-infrared spectroscopy

1 | INTRODUCTION

Cerebrovascular disease (CVD) is the fifth most common cause of mortality in the United States (0.14 million in 2017) [1, 2], and the second worldwide (17.6 million in 2016) [3]. Risk factors for CVD include aging, atherosclerosis, smoking, hypertension, high cholesterol and diabetes [4–7]. Among others, aging represents the major risk factor for the development of CVD. Diagnosis of CVD at early stages is essential for preventing sequential complications. Ideal diagnostic tests should be noninvasive, low-cost, and have high diagnostic accuracy for CVD in early stages of the disease.

CVD is often associated with abnormal microvasculature and tissue dysfunction in the brain, which may impact cerebral-autoregulation (CA) [8, 9]. CA is a physiological mechanism maintaining stable cerebral blood flow (CBF) within a certain range of blood pressure variations [9, 10]. The main regulatory mechanisms of CA are the metabolic, endothelial, myogenic and neurogenic functions that regulate blood flow and tissue oxygenation [11, 12], as well as carbon dioxide partial pressure, hypocapnia and hypercapnia [12]. Disturbances in any one of these components would impact CA, as has been shown in diabetic patients [13, 14]. If the extent of disruption of CA is severe enough, it can also lead to overt tissue injury including microinfarction and microhemorrhages [13]. While there are many other causes of CVD, such as thromboembolic events, vasculitic changes, vascular malformations, or deficiencies in venous drainage, disturbances in CA appear to be the primary driver of cerebral small vessel ischemic changes that contribute significantly to total CVD burden.

While many different methods have been developed to study CA, there is no agreed upon “gold-standard” method for noninvasive evaluation of CA [15–18]. CA has been assessed by quantifying the relationships (gains) of spontaneous low-frequency oscillations (LFOs)

between the mean arterial pressure (MAP) and cerebral hemodynamic parameters such as CBF and cerebral blood oxygenation [19]. In general, smaller LFO gains correspond to better CAs [20, 21]. Although the origin of LFOs remains controversial in the literature, studies have found that the endothelial, neurogenic, and myogenic controls are the main mechanisms responsible for maintaining CBF constant during blood pressure fluctuations [22]. Previous studies have classified LFOs into four frequency intervals: I (0.005–0.0095 Hz), II (0.0095–0.02 Hz), III (0.02–0.07 Hz) and IV (0.07–0.2 Hz) [23–29]. Interval-I and interval-II reflect respectively nitric oxide (NO) dependent and independent endothelial metabolic activities [24, 26, 27]. Interval-III and interval-IV correspond, respectively, to neurogenic and myogenic related metabolic activities [23, 28, 29].

In the study of LFOs, MAP is often monitored by a noninvasive and continuous finger plethysmography technique, which was used in this study. Functional MRI has been used to image cerebral hemodynamics with high spatial resolution, although the high cost, low sampling rate, and nonportability limits its frequent use. Transcranial Doppler ultrasound (TCD) has been used to measure cerebral blood flow velocity (CBFV) in major arteries, which may not be consistent with CBF in the microvasculature [30]. Also, TCD cannot be performed in ~10% of subjects who do not have adequate acoustic windows [31]. Near-infrared spectroscopy (NIRS) provides a noninvasive, rapid, portable, and low-cost alternative for continuous monitoring of cerebral blood oxygenation in the microvasculature, although it does not directly measure CBF [32]. Since CBF and cerebral blood oxygenation are usually coupled and interactive, it is desirable to measure both quantities and investigate their complex relationship.

TCD/NIRS has been used to measure LFOs in CBFV/cerebral blood oxygenation for CA assessment [33–36]. Different orthostatic protocols were applied to induce MAP fluctuations for evaluating dynamic CA including a

sit-stand maneuver [37] and tilting bed. [33] The selected LFO frequency intervals varied in different studies [26, 34, 36, 37], and study cohorts included age-matched older healthy subjects and patients with symptomatic carotid occlusion, ischemic stroke, or Alzheimer disease (AD) [21, 35, 38, 39]. Previous studies have found that CAs (associated with LFO gains) were impaired in patients with symptomatic carotid occlusion or ischemic stroke [21, 38, 39], but preserved in patients with AD [35].

Previously, we conducted a preliminary study in young healthy subjects using an innovative hybrid NIRS /diffuse correlation spectroscopy (DCS) instrument to simultaneously quantify LFOs of CBF and cerebral blood oxygenation at rest, during and after 70° head-up-tilting (HUT) [22]. The hybrid instrument consists of a laboratory-made DCS device for CBF measurements and a commercial frequency-domain NIRS device (Imagent, ISS) for cerebral blood oxygenation measurements including oxy-hemoglobin and deoxy-hemoglobin concentrations ([HbO₂] and [Hb]). HUT was performed to enhance LFOs at ~0.1 Hz. The protocol of 70° HUT has been widely used to induce MAP variation and challenge CA in previous studies [40–43], including ours [22, 44]. This is a standard clinical protocol used to evaluate orthostatic hypotension and vagal reflex integrity. The 70° HUT is sufficient to elicit a maximal response (comparable to 90° HUT). Lesser angles can significantly dampen the cardiovascular response. Results from our pilot study demonstrated the feasibility and reliability of using NIR diffuse optical technologies to simultaneously quantify LFOs of multiple cerebral hemodynamic parameters including CBF, [HbO₂] and [Hb] [22].

This study used the hybrid NIRS/DCS instrument to simultaneously detect LFOs of cerebral hemodynamics in cognitively healthy older subjects with high- or low-risk for developing CVD. Cerebral hemodynamic data were continuously collected at rest, during, and after 70° HUT. LFO intensities were extracted from the measured variables (MAP, CBF, [HbO₂] and [Hb]) using power spectral analyses in four frequency intervals (interval-I - interval-IV) [23–29]. The LFO transfer function gains were quantified by transfer function analyses with MAP as the input and cerebral hemodynamic variables (CBF, [HbO₂] and [Hb]) as the outputs [22]. Thus, the extent of oscillatory changes in MAP as a continuous variable were associated with CA responses that varied on a continuous scale to effectively control and regulate MAP oscillatory changes (eg, lowering transfer function gain) [20, 21, 23, 35, 37, 45]. Since LFO gains correlate inversely with the CAs [20, 21], we hypothesized that they can be used as biomarkers for diagnosis of CVD at early stages, that is, distinguishing two groups of subjects, who were classified into high- or low-risk for developing CVD based on Framingham risk score (FRS).

2 | MATERIALS AND METHODS

2.1 | Participants

This study was approved by the University of Kentucky (UK) Institutional Review Board (IRB). The written IRB consent was obtained from each subject before participation. Twenty-six cognitively healthy older adults (23 females and 3 males) with a mean age of 77.7 ± 6.8 years (mean \pm SD) were recruited from a well-characterized aging cohort, followed by the Alzheimer's Disease Center (ADC) at the UK Sanders-Brown Center on Aging. Subjects with at least one of the following criteria were excluded from the study: unstable cardiac diseases, orthostatic symptoms during upright standing, non-CVD causes of cognitive decline and AD risk factors, such as APOE4 allele, atrial fibrillation and other coexisting brain disorders.

The level of individual's risk for developing CVD was evaluated based on clinical diagnosis by neurologists and ADC databases. The FRS was adapted to predict CVD over 10 years including gender, age, history of diabetes, blood pressure, smoking and cholesterol level. [46, 47] The scoring scale of Framingham ranged from 1 to 30 points. The 26 subjects with risks for CVD were classified into two groups based on the FRS cutoff of 15-points: low-risk group (FRS ≤ 15 , $n = 14$) and high-risk group (FRS > 15 , $n = 12$).

2.2 | Experimental protocols

Following our established experimental protocol [22], the participant was asked to lie in a supine-position on a tilting bed (Hausmann). Two Velcro strips were used (one over the chest and another over the knee) to protect the subject from falling during HUT (Figure 1A). A hybrid NIRS/DCS probe (Figure 1B) was fixed with a medical tap on the middle of the forehead about 1 cm above the eyebrows to avoid frontal air sinuses. Another layer of elastic bandage was wrapped around the subject's head to secure the probe and eliminate the influence of ambient light. The hybrid optical probe was connected to the hybrid NIRS/DCS instrument for cerebral hemodynamic monitoring (Figure 1C). A finger photoplethysmography sensor (Portapres, Netherlands), calibrated by a regular pressure-cuff on the subject's upper arm, was used to record MAP noninvasively and continuously. MAP was calculated using the software package provided by the manufacturer. Optical data were continuously recorded by the hybrid NIRS/DCS instrument throughout the entire experimental protocol, which included a 10 minutes baseline at rest, 10 minutes HUT (70°) and 10 minutes recovery after HUT back to 0°.

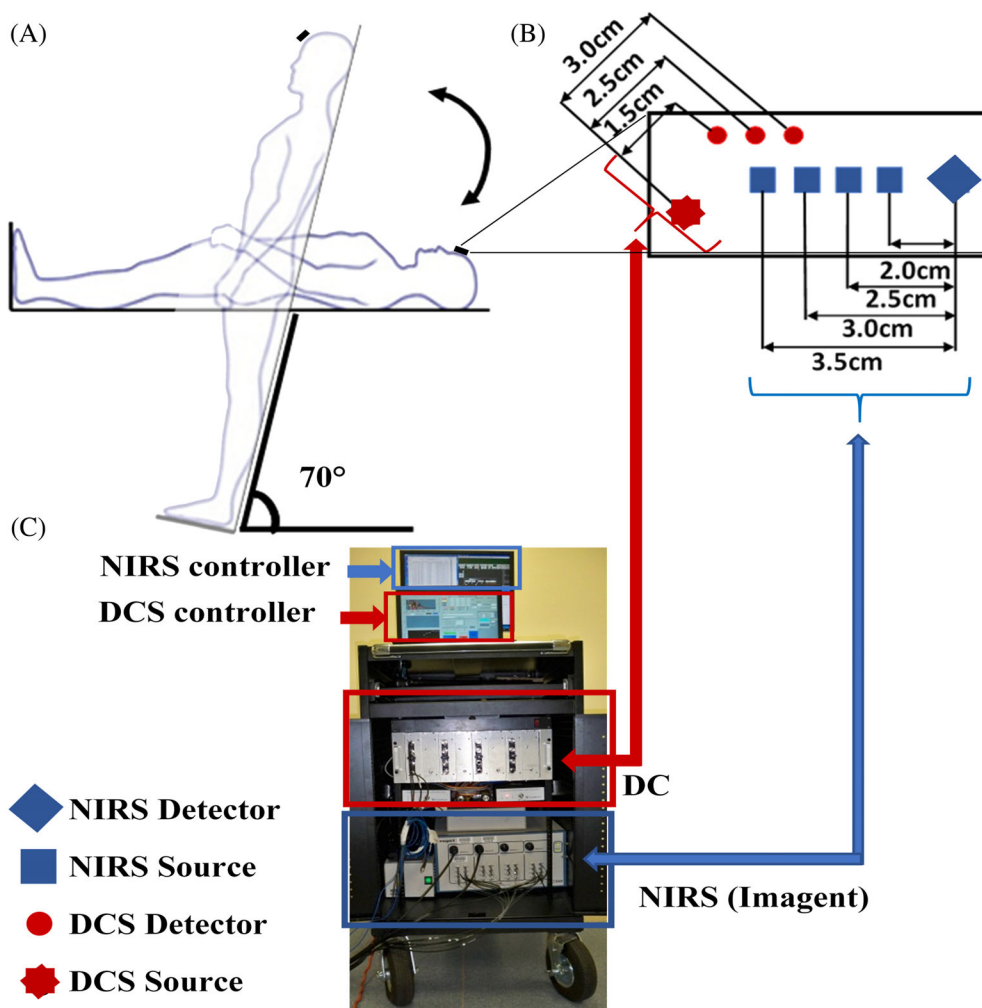


FIGURE 1 A hybrid NIRS/DCS instrument for continuous and simultaneous measurements of $\Delta[\text{HbO}_2]$, $\Delta[\text{Hb}]$ and relative change in CBF (rCBF) before, during and after head-up-tilting (HUT). A, Illustration of a titling bed, and baseline, HUT, and recovery positions. B, A hybrid NIRS/DCS probe with multiple source-detector (S-D) separations. C, A hybrid instrument integrating a commercial NIRS device (Imagent, ISS) and a laboratory-made DCS device. CBF, cerebral blood flow; DCS, diffuse correlation spectroscopy; Hb, deoxy-hemoglobin concentration; HbO_2 , oxy-hemoglobin concentration; NIRS, near-infrared spectroscopy

A physician stayed at the bedside of the testing room for safety monitoring during experiments.

2.3 | Hybrid NIRS/DCS instrument for $[\text{HbO}_2]$, $[\text{Hb}]$ and CBF measurements

Details about our innovative hybrid NIRS/DCS instrument for simultaneous measurements of $[\text{HbO}_2]$, $[\text{Hb}]$ and CBF have been reported previously [22]. Briefly, a commercial frequency-domain NIRS device (Imagent, ISS) was used for cerebral blood oxygenation measurements. The Imagent device measured changes in amplitudes and phases of frequency-modulated light (110 MHz) at two wavelengths (690 and 830 nm, <10 mW) resulting from tissue absorption and scattering using four source-detector (S-D) with separations of 2.0, 2.5, 3.0 and 3.5 cm. A simplified solution based on a semi-infinite geometry for the photon diffusion equation revealed linear relationships between the measured phases and logarithmic amplitudes vs multiple S-D separations. The wavelength-dependent tissue absorption

coefficient μ_a and reduced scattering coefficient μ_s' were then extracted by fitting the slopes of these linear relationships. The absolute baseline values of $[\text{HbO}_2]$ and $[\text{Hb}]$ were calculated from the measured μ_a at the two wavelengths. However, phase slopes over multiple S-D separations were not used in the present analysis due to the low signal-to-noise ratio (SNR) and instable phase slopes, although future studies with improved NIRS systems would allow an evaluation of scattering changes that may result from HUT. As such, cerebral oxygenation concentration was computed depending on the amplitude data of the two wavelengths from a single S-D separation (2.5 cm). Relative changes in cerebral blood oxygenation (ie, $\Delta[\text{HbO}_2]$ and $\Delta[\text{Hb}]$) were then calculated based on the modified Beer-Lambert law [48, 49], where the differential pathlength factor was derived from the literature [50, 51].

A laboratory-made DCS device was used for CBF measurement [22, 52–54]. The DCS device used a long-coherence laser diode at 830 nm (100 mW, CrystaLaser) as the source and 16 single-photon-counting avalanche photodiode detectors (APDs, PerkinElmer) as the

detectors with S-D separations of 1.5, 2.5 and 3.0 cm. The laser diode transmitted long-coherent light through a source fiber (diameter = 200 μm) into the tissue. The APDs detected temporal light intensity fluctuations in a single speckle area on the tissue surface through single-mode fibers (core diameter = 5.6 μm), resulting primarily from the motions of red blood cells in the microvasculature (ie, CBF). Signals collected by eight APDs at the S-D separation of 2.5 cm were averaged to improve the SNR. The relative change in CBF (rCBF) was calculated by normalizing data to its baseline value (assigned to be 100%) before HUT. The tissue optical properties (μ_a and μ_s') used for the present computation of CBF index were derived from prior studies reported in the literature to be optimal for such assessments [55].

The laser diodes for DCS and Imagent measurements were turned on alternately to avoid the light interference between the flow and oxygenation measurements. The acquisition time for collecting one frame of cerebral hemodynamic data was ~ 1.4 seconds (equivalent to a sampling rate $f_s = 0.7$ Hz), which included ~ 0.8 seconds for Imagent measurement, ~ 0.5 seconds for DCS measurement, and ~ 0.1 seconds for switching between the two measurements.

2.4 | Extraction of LFO intensities/ power spectral densities

LFO intensities of MAP, rCBF, $\Delta[\text{HbO}_2]$ and $\Delta[\text{Hb}]$ under three physiological conditions (ie, at rest, during HUT and during recovery after HUT) are extracted from their power spectral densities (PSDs), calculated by Welch's method [22]. Briefly, 10 minutes time course dataset under each physiological condition (~ 420 data points at the sampling rate $f_s = \sim 0.7$ Hz) is first detrended to remove the baseline shift. The detrended data are divided into eight segments with 50% overlap in two adjacent segments, producing a data length of ~ 93 ($420 \times 2/9$) points for each segment. The $\text{PSD}_x(f)$ and $\text{PSD}_y(f)$ are generated by MATLAB function of "pwelch." Here, x denotes to the MAP signal, y denotes to other physiological signals (CBF, $[\text{HbO}_2]$ and $[\text{Hb}]$), and f is the frequency with a resolution of ~ 0.0075 Hz ($f_s/93$) in the range of 0.005 to 0.2 Hz. The cross-spectral density $\text{CSD}_{xy}(f)$ is calculated by MATLAB function of "cpsd."

2.5 | Assessment of LFO gain and CA

CA has been assumed to be a linear system with MAP as the input and cerebral hemodynamic parameters as the outputs. This assumption indicates that the CA is

controlling the relationship between MAP and CBF to maintain an adequate CBF value within a range of MAP variations (~ 50 – ~ 150 mm Hg) [56–58]. Prior studies have demonstrated that CA can be indirectly assessed by examining the relationship between MAP and hemodynamic parameters, that is, how the MAP oscillation amplitude changes are transmitted to the cerebral hemodynamics parameters [20, 21, 23, 35, 37, 45]. Such techniques examine the gain of LFO using only a single hemodynamic measurement. In the present study, the hybrid NIRS/DCS technique allows assessment of LFO gains with multiple functional parameters across four physiological processes related to: (a) nitric oxide independent and (b) dependent endothelial activities, (c) neurogenic activities and (d) myogenic activities [23–29]. As such, the present techniques provide a more direct and comprehensive assessment of CA than is afforded using traditional methodologies.

The gain $G(f)$ of a linear system is quantified by transfer function analysis between the $\text{CSD}_{xy}(f)$ that was derived from the PSD of the MAP (PSD_{xx}) and cerebral hemodynamic (PSD_{yy}) signals $G(f) = \frac{\text{CSD}_{xy}(f)}{\text{PSD}_{xx}(f)}$ [18, 22, 38, 59–61]. Based on the mentioned physiological processes [23–29], $G(f)$ is classified into four frequency intervals: interval-I = 0.005 to 0.095 Hz, interval-II = 0.095 to 0.02 Hz, interval-III = 0.02 to 0.07 Hz and interval-IV = 0.07 to 0.2 Hz. The mean value of $G(f)$ in each frequency interval is calculated as a biomarker to assess CA: $\text{CA} \propto 1/G(f)$ [20, 21].

The CA evaluation based on the LFO depends on the relation between the frequency oscillation of the MAP and the cerebral hemodynamic response. In our study, we cover very LFOs (eg, interval I: 0.005–0.095 Hz) that are related to the NO activities [62]. This means only several oscillation circles within 10 minutes [62]. Accordingly, a long-time period should be considered to transmit the oscillatory components of the NO in the hemodynamic signal. [62, 63] In addition, accurate measurement of dynamic CA response is dependent on achieving a stable MAP that allows for stable change in cerebral hemodynamic response. Prior studies have demonstrated that 10 minutes duration acquisitions at each bed position are optimal for stable data collection [64].

2.6 | Statistical analysis

The statistical analysis was performed for both time-course and LFO data utilizing Independent t tests and Wilcoxon signed ranks tests by IBM SPSS (SPSS 2019). Independent t tests are conducted to test intergroup differences between the two groups at each frequency interval under each physiological condition. Wilcoxon signed

ranks tests are performed to test the intragroup differences between the baseline and other physiological conditions (ie, during and after HUT). A P -value of $<.05$ is considered significant.

3 | RESULTS

3.1 | Subject characteristics and valid measurements

Although 26 cognitively healthy older subjects (23 females and 3 males) were measured, one female subject from the high-risk group was excluded from data analysis due to failure of optical measurements. One male subject from the low-risk group was also excluded due to the occurrence of syncope during HUT. The remaining subjects ($n = 24$) were divided into low-risk ($n = 13$) and high-risk ($n = 11$) groups based on FRS (Figure 2). In addition, one female subject from the low-risk group had an abnormal MAP measurement during the recovery. Accordingly, 13 female subjects (73.0 ± 4.3 years) were included in the low-risk group for data analysis (13 at baseline, 13 during HUT, and 12 after HUT for recovery). Nine females and two males (84.2 ± 4.0 years) were included in the high-risk group ($n = 11$). The significant difference in age between the two groups ($P < .001$) had been considered in FRSs.

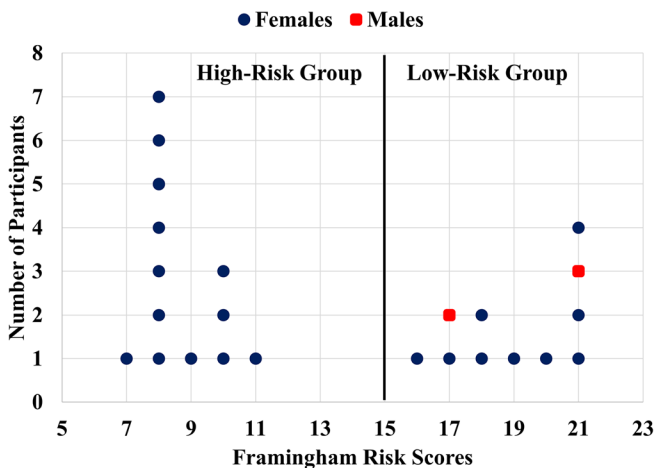


FIGURE 2 The Framingham risk score (FRS) distribution. The study participants with valid data were divided into two groups: low- and high-risk for developing cerebrovascular disease (CVD). The FRS less or equal to 15 was considered as a low-risk group, otherwise was considered as a high-risk group for developing CVD

3.2 | Time-course cerebral hemodynamic responses to HUT

Figure 3 shows the time-course data taken from two subjects with high- or low-risk for CVD before, during, and after HUT. All measured parameters at the resting baseline were relatively stable. As expected, rCBF decreased during HUT due to the decrease of cardiac output and the increase of cerebral vasculature resistance induced by the orthostatic stress. The reduced rCBF affected oxygen delivery, thus led to variations in $\Delta[\text{HbO}_2]$ and $\Delta[\text{Hb}]$. Most of subjects (22 out of 24) had a trend similarly to these two subjects. However, two subjects in the low-risk group exhibited an increase in rCBF (data not shown). After recovery, all measured physiological parameters tended to return to their baseline levels.

3.3 | Intergroup and intragroup differences in cerebral hemodynamic responses

Figure 4 shows the mean values of time-course results for all parameters (MAP, rCBF, $\Delta[\text{HbO}_2]$ and $\Delta[\text{Hb}]$) at the three-bed positions (baseline, HUT, and recovery). The results were divided into overall changes for all subjects, low-risk group, and high-risk group. In general, MAP and rCBF results were more stable compared to the oxygenation data. The MAP intragroup results showed significant changes during HUT and back to the baseline level for all subgroups and overall group (marked with $\$$ and P values in Figure 4, Wilcoxon signed ranks test). However, the intergroup difference was only significant at baseline and recovery (marked with $*$ and P values in Figure 4, independent t test). The rCBF intragroup results were significant during HUT and recovery for all subjects and the high-risk subgroup only. The intergroup result of the rCBF was only significant during HUT. The intragroup results of $\Delta[\text{Hb}]$ were statistically relevant for all groups during recovery only, and there is no intergroup significance for $\Delta[\text{Hb}]$, while $\Delta[\text{HbO}_2]$ did not show any significant changes at all.

3.4 | Low-frequency oscillations of MAP, rCBF, $\Delta[\text{HbO}_2]$ and $\Delta[\text{Hb}]$

Figure 5 shows the PSD data calculated from the same two subjects with high- or low-risk for CVD (Figure 3). For both subjects, PSDs of MAP, rCBF, $\Delta[\text{HbO}_2]$ and $\Delta[\text{Hb}]$ varied during HUT and recovered toward their baseline levels after HUT.

FIGURE 3 Illustrative time-course responses of mean arterial pressure (MAP) (mmHg), relative change in CBF rCBF (%), $\Delta[\text{HbO}_2]$ (μM) and $\Delta[\text{Hb}]$ (μM) in two subjects, measured continuously at resting baseline (10 minutes), during HUT (10 minutes), and after HUT for recovery (10 minutes). A, A 68-years-old female subject with low-risk for developing CVD. B, A 84-years-old female subject with high-risk for developing CVD. CBF, cerebral blood flow; CVD, cerebrovascular disease; Hb, deoxy-hemoglobin concentration; HbO_2 , oxy-hemoglobin concentration; HUT, head-up-tilting

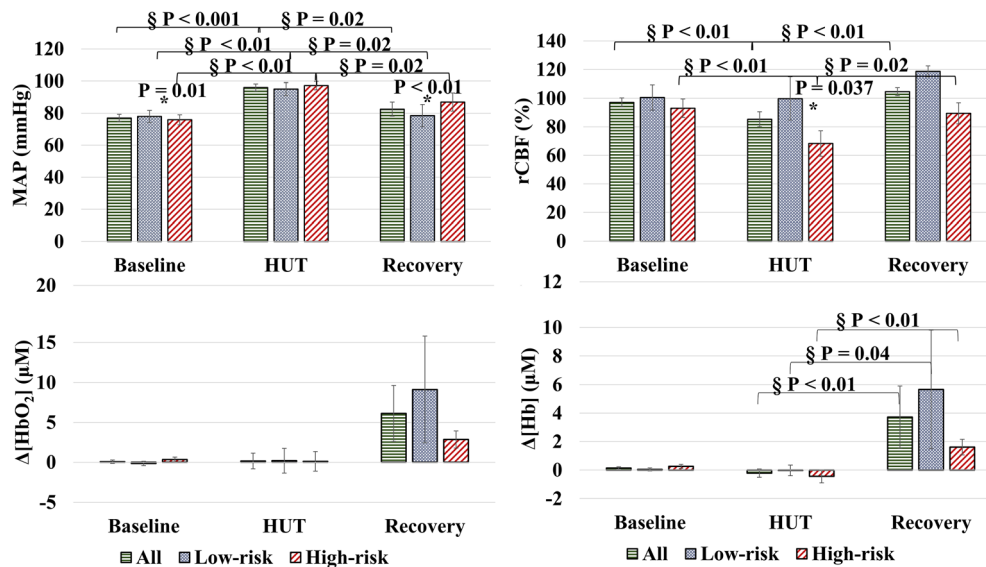
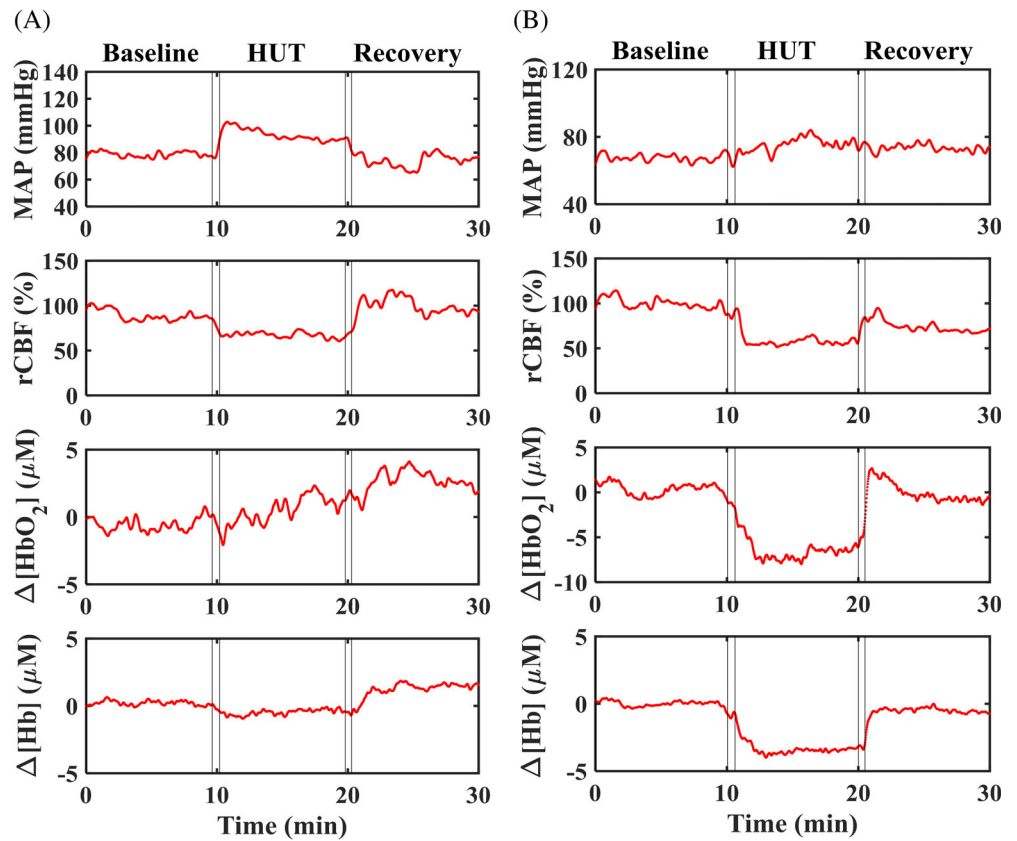


FIGURE 4 The time-course mean values of cerebral hemodynamic parameters. The figure shows the mean values of each hemodynamic parameter (MAP, rCBF, $\Delta[\text{HbO}_2]$, and $\Delta[\text{Hb}]$) at the three-bed positions (baseline, HUT, and recovery). § denotes for a significant result of the intragroup using the Wilcoxon signed ranks test; the P -values are marked in the figure. * denotes a significant result between the two groups using the independent t test. MAP showed significant changes between the two groups at baseline and recovery. rCBF showed a significant result between the two groups during the HUT. The cerebral oxygenation results did not show any significance between groups. CBF, cerebral blood flow; MAP, mean arterial pressure; Hb, deoxy-hemoglobin concentration; HbO_2 , oxy-hemoglobin concentration; HUT, head-up-tilting; rCBF; relative change in CBF

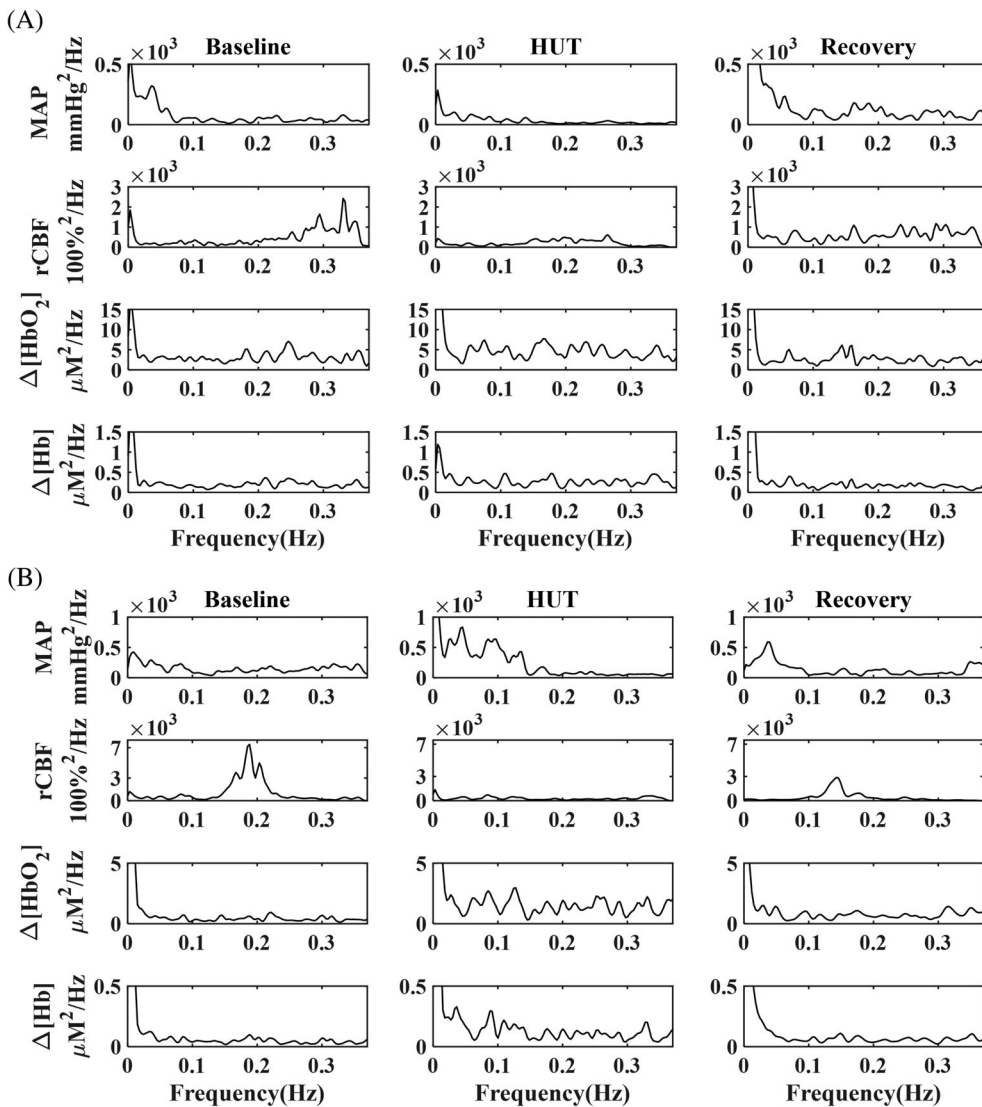


FIGURE 5 Low-frequency oscillation (LFO) intensities of mean arterial pressure (MAP), relative change in CBF (rCBF), $\Delta[\text{HbO}_2]$ and $\Delta[\text{Hb}]$ in two subjects before, during and after head-up-tilting (HUT). A, A 68-years-old female subject with low-risk for developing CVD. B, A 84-years-old female subject with high-risk for developing CVD. CBF, cerebral blood flow; CVD, cerebrovascular disease; Hb, deoxy-hemoglobin concentration; HbO₂, oxy-hemoglobin concentration

3.5 | Intergroup and intragroup differences in LFO gains

Figure 6 shows the mean LFO gain values of all parameters (MAP, rCBF, $\Delta[\text{HbO}_2]$ and $\Delta[\text{Hb}]$) in four frequency intervals (interval-I - interval-IV) for two groups (high- or low-risk for CVD) under three physiological conditions (at rest, during, and after HUT).

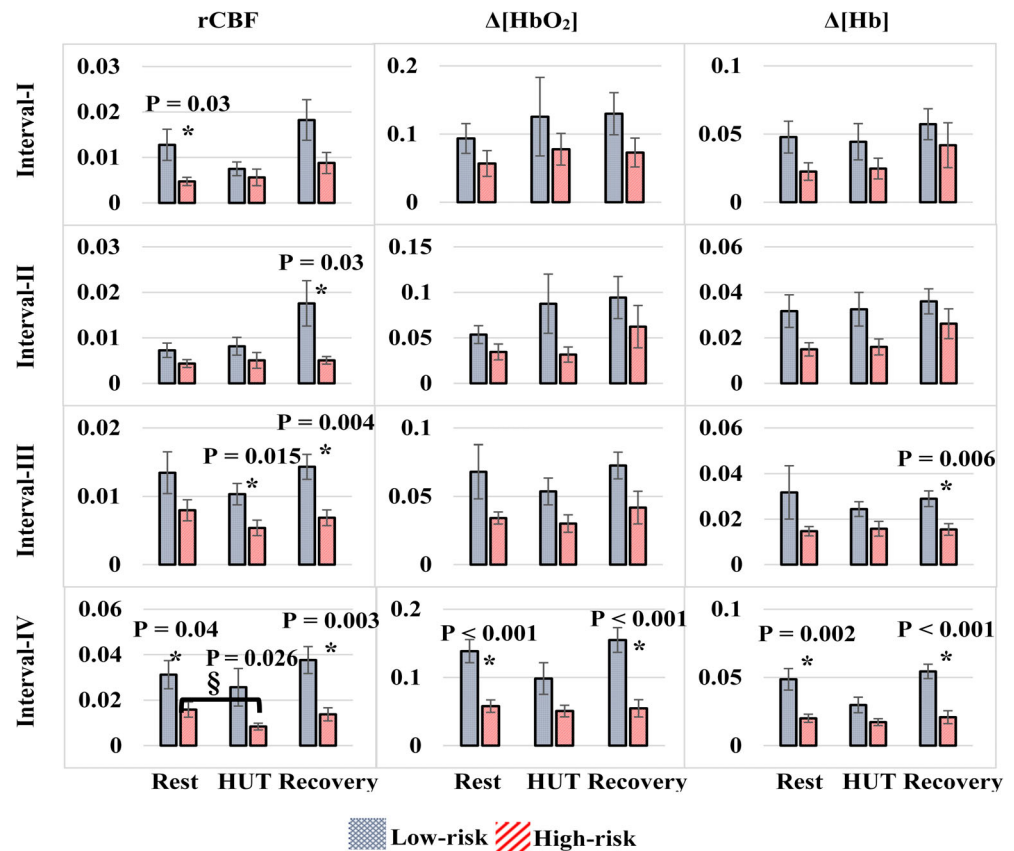
Overall, all LFO gains in the high-risk group were lower than those in the low-risk group, although only some intergroup gain difference reached significance (marked with * and *P* values in Figure 6, independent *t* test).

During HUT, intragroup gains at interval-I and interval-II varied (increased or decreased) from their resting baselines. However, most of intragroup gains at interval-III and interval-IV reduced, except that the gain of $\Delta[\text{Hb}]$ at interval-III in the high-risk group elevated slightly.

Moreover, HUT-induced gain reductions in the high-risk group are generally smaller than those in the low-risk group, although most of these intragroup gain reductions did not reach significance, except the rCBF gain reduction at interval-IV in the high-risk group (marked with § and *P* value in Figure 6, Wilcoxon signed ranks test). During recovery, most of LFO gains did not completely recover to their baseline levels, except those at interval-IV.

Interestingly, intragroup and intergroup gain variations across all measured cerebral variables (ie, rCBF, $\Delta[\text{HbO}_2]$ and $\Delta[\text{Hb}]$) at interval-IV were highly consistent. LFO gains decreased during HUT and recovered to their baselines after HUT. Significant intergroup gain differences were observed at rest and during recovery. Moreover, the HUT caused smaller intragroup gain reductions in the high-risk group compared to the low-risk group, which changed the intergroup gain

FIGURE 6 Low-frequency oscillation gains of mean arterial pressure (MAP), relative change in CBF (rCBF), $\Delta[\text{HbO}_2]$ and $\Delta[\text{Hb}]$ in four frequency intervals (interval-I - interval-IV) for two groups (high- or low-risk for cerebrovascular disease [CVD]) under three physiological conditions (at rest, during resting baseline, head-up-tilting [HUT], and recovery). § denotes for a significant result of the intragroup using the Wilcoxon signed ranks test; the P -values are marked in the figure. * indicates significant differences in intergroup gains (independent t test). CBF, cerebral blood flow; Hb, deoxy-hemoglobin concentration; HbO_2 , oxy-hemoglobin concentration



differences from significant at rest to insignificant during HUT.

4 | DISCUSSION AND CONCLUSIONS

4.1 | Study innovations

The goal of the present study is to test whether LFO gains of cerebral hemodynamic variables, quantified by our innovative hybrid optical instrument, are useful biomarkers to distinguish two groups of cognitively healthy older subjects with high- or low-risk for developing CVD. Upon comparison with literature [21, 26, 33–39], we believe this study is innovative in that: (a) it used an innovative hybrid optical instrument to simultaneously measure multiple cerebral hemodynamic parameters including rCBF, $\Delta[\text{HbO}_2]$ and $\Delta[\text{Hb}]$ in cerebral microvasculature. Multiple cerebral functional parameters provided more comprehensive assessment of brain activities than a single parameter alone, (b) it studied a unique population: cognitively healthy older subjects stratified by cerebrovascular risk and (c) it innovatively explored CAs (extracted from LFO gains of cerebral

hemodynamics) as new biomarkers for diagnosis of CVD at preclinical stage.

4.2 | Interpretation of cerebral hemodynamic responses to HUT

The time-course results of all parameters (Figure 4) showed less variations during the orthostatic stress for MAP and rCBF compared to the oxygenation data ($\Delta[\text{HbO}_2]$ and $\Delta[\text{Hb}]$). The high variations of oxygenation data during orthostatic stress may attribute to the various oxygenation compensatory mechanisms that could be strongly maintain the adequate cerebral oxygenation level, for example, the ability of the brain to produce oxygen as a compensatory mechanism [45]. Studies have shown that during cerebral activities, CBF is not necessarily coupled to the cerebral metabolic rate of oxygen consumption (CMRO_2), or CBF may be connected nonlinearly to CMRO_2 . That means, even with increasing of CBF, which is the primary source of oxygen delivery to the brain, still the CMRO_2 is required. [65, 66] Another compensatory mechanism for hypoxia due to hypoperfusion is to increase the oxygen extraction coefficient from blood [67]. We noticed the rCBF of two subjects were increased during HUT as unfavorable

outcomes which may due to the subjects were not respond to the HUT [68].

4.3 | Interpretation of intergroup and intragroup differences in LFO gains/CAs

At the resting baseline before HUT, all LFO gains in the high-risk group were relatively lower than those in the low-risk group (Figure 6). Particularly, significant intergroup gain differences were observed in all measured cerebral variables (rCBF, $\Delta[\text{HbO}_2]$ and $\Delta[\text{Hb}]$) at interval-IV and in rCBF at interval-I. The relatively lower gains observed in the high-risk group may attribute to enhanced steady-state cerebrovascular reactivity, metabolic reserve, or oxygen diffusion [23, 37, 69, 70], which act as compensatory mechanisms to maintain the CA. HUT generated MAP fluctuations to challenge the CA. As a result, intragroup gains at interval-I and interval-II fluctuated (increased or decreased) from their resting baselines. However, most of intragroup gains at interval-III and interval-IV were reduced, suggesting potentially stronger dynamic CAs during HUT compared to rest. Moreover, HUT-induced gain reductions at interval-III and interval-IV in the high-risk group are generally smaller than those in the low-risk group, suggesting potentially weaker dynamic CAs during HUT in this high-risk group [30].

Interestingly at interval-IV, HUT-induced intragroup and intergroup gain variations were highly consistent across all measured cerebral variables (i.e., rCBF, $\Delta[\text{HbO}_2]$ and $\Delta[\text{Hb}]$): LFO gains decreased from their baselines during HUT and recovered to their baselines after HUT. Moreover, intergroup gain differences were significant at rest and during recovery. However, all intergroup gain differences became insignificant during HUT due to different degrees of intragroup gain reductions. These results confirmed weaker dynamic CAs (corresponding to smaller gain reductions) during HUT in the high-risk group compared to the low-risk group.

We speculate from these results that cerebrovascular risk affects primarily neurogenic and myogenic activities to regulate CA, as interval-III and interval-IV correspond respectively to neurogenic and myogenic related metabolic activities [23, 28, 29]. This speculation is supported by other studies in aging populations where neurogenic and myogenic activities at interval-III and interval-IV were the substantial regulatory factors for the CA in contrast to endothelial activities at interval-I and interval-II [26, 34]. In addition, cerebrovascular risk seems affecting rCBF more than $\Delta[\text{HbO}_2]$ and $\Delta[\text{Hb}]$, as more intergroup and intragroup differences were observed in rCBF than other two variables (Figure 6).

One important finding from this study is that cerebrovascular risk alters steady-state and dynamic CAs

differently in cognitively healthy older subjects. As a result, the high-risk group has stronger CA at rest but weaker dynamic CA during HUT. In other words, compared to the low-risk group, the high-risk group demonstrated maximum efforts to control CA at resting state via underlying brain compensatory mechanisms. During HUT, this compensatory mechanism appears to be insufficient to maximize CA. These results are compatible with our overall hypothesis that CA in high risk individuals is capable of maintaining cerebral hemodynamics in an unchallenged state, but the demonstrated failure to compensate at times of stress may be ultimately responsible for the development of CVD that accumulates over time.

Interestingly, previous studies have observed that CAs were impaired in patients with symptomatic carotid occlusion or ischemic stroke [21, 38, 39], but preserved in patients with AD [35]. Accordingly, one potential future application is to use the innovative technologies/protocols established in this study to investigate the differences in CAs as biomarkers to differentiate subjects under different conditions such as high-risk for CVD, CVD (eg, symptomatic carotid occlusion or ischemic stroke), AD, and CVD plus AD. It is crucial to know whether the cognitive deficit is caused by AD or by related vascular problem, so that clinicians can make effective treatment plan accordingly. Unlike AD, there are treatments available for controlling vascular conditions.

4.4 | Study challenges and limitations

One major limitation of this study is the small number of subjects, which affects our statistical analyses and study power. In addition, we recruited subjects based on FRS and did not prespecify sex as a recruitment characteristic. This could introduce a sex-specific selection bias, which will need to be addressed in future studies. The FRS, used to stratify participants in the present study, is a well-established tool for assessing CVD risks in the population. It has been shown to correlate well with imaging measures of CVD, however there are limitations to its use in the present study. First, our participants do not have evidence for current symptomatic CVD. Second, the FRS model was developed to allow the prediction of stroke or heart attack over a 10 years period, and therefore may not reflect the actual CVD status of the participants at the time of the study [71]. Such limitations need to be considered in the interpretation of the present data and for the future development of biomarkers examining preclinical CVD.

Moreover, the methodology—simultaneously measure multiple cerebral hemodynamic parameters with the hybrid optical instrument during HUT to identify new

biomarkers (LFO gains) for diagnosis of CVD at preclinical stage, is very unique to compare with other results. The NIRS/DCS sources and detectors were arranged in the way to avoid light interference between the NIRS and DCS measurements (Figure 1B). This may result in a small discrepancy between the two measurements due to tissue hemodynamic heterogeneity. This limitation may be overcome in the future by using optical filters in front of the NIRS/DCS detectors to reduce such interference, so that NIRS/DCS sources and detectors cover the same region. The S-D separation of 2.5 cm that has been broadly utilized in NIRS/DCS studies to quantify CBF and cerebral oxygenation variations in adult brain cortices with adequate SNRs [22, 44, 72, 73]. However, the collected cerebral signals were inherently influenced by the partial volume effect of overlayer tissues (scalp and skull) [22, 74]. In the future, multi-layer models with measurements at multiple S-D separations may be adapted to reduce the partial volume effect [75–79].

The sampling frequency of the hybrid NIRS/DCS instrument is relatively low (0.7 Hz), which limits the extraction of LFOs in other intervals with higher frequencies such as respiration (0.15–0.5 Hz) and cardiac (0.5–2 Hz) activities [28, 80, 81]. To improve the sampling rate of optical measurements, we recently worked on a fast DCS technique using a software correlator (instead of a conventional hardware correlator) [82] to create a frame of CBF measurement within only 0.05 seconds. We also explored adding a 785 nm notch filter in front of the Imagent detector so that both DCS and Imagent data were collected concurrently without light interference across the two measurements. With these improvements, the sampling frequency of NIRS/DCS measurements reached 10 Hz.

While HUT creates orthostatic stress to challenge the CA, it may also cause syncope, as observed from one participant in this study. We are currently exploring other noninvasive stimuli (eg, memory tests, CO₂ inhalations) for challenging the CA to avoid syncope during HUT. Ultimately, we expect to study more subjects with the improved instrument and experimental protocols in the future to draw solid conclusions.

5 | CONCLUSIONS

A novel hybrid NIRS/DCS instrument was successfully used to simultaneously detect LFOs of MAP, CBF, [HbO₂] and [Hb] in cognitively healthy older subjects with high- or low-risk for developing CVD. The intragroup and intergroup differences in LFO gains were characterized to evaluate CA differences between the low-risk and high-risk groups as CAs correlate inversely with LFO gains.

The present data suggest that rCBF may be sufficient for early detection of CVD based on the significant associations of this measurement with CVD classification over the four frequency intervals. However, the multi-parameter measurements correlated with the orthostatic stress for challenging CA and LFO analysis may also provide critical insights in future experiments using alternate CA stress challenges. We also note that the multiple parameters measured in the present study provide additional information beyond that obtained through measurement of rCBF alone. While the rCBF contributions to the four frequency intervals (I–IV) showed the greatest statistical significance overall, measurements of cerebral oxygenation demonstrated greater statistical significance at interval-IV compared to rCBF. These data demonstrate that measurement of cerebral oxygenation might serve as a biomarker of myogenic activity, albeit only at interval-IV. Furthermore, the significant outcomes of multiple functional parameters (rCBF, [HbO₂] and [Hb]) confirmed that the neurogenic and myogenic activities (intervals III and IV) had more contribution to the CA compared to the endogenous activities (intervals I and II).

Taken together, LFO gains of cerebral functional parameters are potentially valuable biomarkers for early diagnosis of CVD based on associations with CAs.

ACKNOWLEDGMENTS

We acknowledge the support from The Higher Committee for Education Development in Iraq, and the advice from Dr Fred Schmitt at the University of Kentucky Alzheimer's Disease Center (ADC) and Dr. Erin Abner at the Department of Epidemiology and Department of Biostatistics, University of Kentucky. This work was partially supported by the National Institutes of Health (NIH, 5P30-AG028383, R21-HD091118, R01-HD101508 and R01-AG062480), American Heart Association (AHA, 16GIA-30820006) and National Science Foundation (NSF, EPSCoR-1539068). The content is solely the responsibility of the authors and does not necessarily represent the official views of the NIH, AHA, or NSF.

ORCID

Ahmed A. Bahrani  <https://orcid.org/0000-0003-1809-0879>

REFERENCES

- [1] K.D. Kochanek, S.L. Murphy, J. Xu, E. Arias, Deaths: Final Data for 2017, National Vital Statistics Reports, U.S. DEPARTMENT OF HEALTH AND HUMAN SERVICES, USA, **2019**, pp. 1–77.
- [2] M. Heron, Deaths: Leading Causes for 2017, *2019*.
- [3] E. J. Benjamin, P. Muntner, A. Alonso, M. S. Bittencourt, C. W. Callaway, A. P. Carson, A. M. Chamberlain, A. R.

- Chang, S. Cheng, S. R. Das, F. N. Delling, L. Djousse, M. S. V. Elkind, J. F. Ferguson, M. Fornage, L. C. Jordan, S. S. Khan, B. M. Kissela, K. L. Knutson, T. W. Kwan, D. T. Lackland, T. T. Lewis, J. H. Lichtman, C. T. Longenecker, M. S. Loop, P. L. Lutsey, S. S. Martin, K. Matsushita, A. E. Moran, M. E. Mussolino, M. O'Flaherty, A. Pandey, A. M. Perak, W. D. Rosamond, G. A. Roth, U. K. A. Sampson, G. M. Satou, E. B. Schroeder, S. H. Shah, N. L. Spartano, A. Stokes, D. L. Tirschwell, C. W. Tsao, M. P. Turakhia, L. B. VanWagner, J. T. Wilkins, S. S. Wong, S. S. Virani, American Heart Association Council on Epidemiology and Prevention Statistics Committee and Stroke Statistics Subcommittee, *Circulation* **2019**, *139*, e56.
- [4] A. J. Catto, P. J. Grant, *Blood Coagul. Fibrinolysis* **1995**, *6*, 497.
- [5] E. V. Backhouse, C. A. McHutchison, V. Cvorov, S. D. Shenkin, J. M. Wardlaw, *Neurology* **2017**, *88*, 976.
- [6] C. Hajat, R. Dundas, J. A. Stewart, E. Lawrence, A. G. Rudd, R. Howard, C. D. Wolfe, *Stroke* **2001**, *32*, 37.
- [7] O. M. Al-Janabi, A. A. Bahrani, G. A. Jicha, Vascular Contributions to Alzheimer's Disease and Mixed Pathological Disease States. in *Alzheimer's Disease*, Avid Science, Telangana, India, **2017**, p. 2.
- [8] R. Zhang, J. H. Zuckerman, K. Iwasaki, T. E. Wilson, C. G. Crandall, B. D. Levine, *Circulation* **2002**, *106*, 1814.
- [9] J. D. Jordan, W. J. Powers, *Am. J. Hypertens.* **2012**, *25*, 946.
- [10] R. Aaslid, K. F. Lindegaard, W. Sorteberg, H. Nornes, *Stroke* **1989**, *20*, 45.
- [11] W. M. Armstead, *Anesthesiol. Clin.* **2016**, *34*, 465.
- [12] A. V. Andersen, S. A. Simonsen, H. W. Schytz, H. K. Iversen, *Neurophotonics* **2018**, *5*, 030901.
- [13] S. Shekhar, S. Wang, P. N. Mims, E. Gonzalez-Fernandez, C. Zhang, X. He, C. Y. Liu, W. Lv, Y. Wang, J. Huang, F. Fan, *Curr. Res. Diabetes Obes. J.* **2017**, *2*, 555587.
- [14] B. N. Mankovsky, R. Piolot, O. L. Mankovsky, D. Ziegler, *Diabet. Med.* **2003**, *20*, 119.
- [15] F. A. Sorond, J. M. Serrador, R. N. Jones, M. L. Shaffer, L. A. Lipsitz, *Ultrasound Med. Biol.* **2009**, *35*, 21.
- [16] L. Rangel-Castilla, J. Gasco, H. J. Nauta, D. O. Okonkwo, C. S. Robertson, *Neurosurg. Focus* **2008**, *25*, E7.
- [17] S. P. Klein, B. Depreitere, G. Meyfroidt, *Crit. Care* **2019**, *23*, 160.
- [18] J. A. Claassen, A. S. Meel-van den Abeelen, D. M. Simpson, R. B. Panerai, International Cerebral-autoregulation Research, *J. Cereb. Blood Flow Metab.* **2016**, *36*, 665.
- [19] K. Tgavalekos, T. Pham, N. Krishnamurthy, A. Sassaroli, S. Fantini, *PLoS One* **2019**, *14*, e0211710.
- [20] J. R. Whittaker, I. D. Driver, M. Venzi, M. G. Bright, K. Murphy, *Front. Neurosci.* **2019**, *13*, 433.
- [21] J. Kwan, M. Lunt, D. Jenkinson, *Blood Press. Monit.* **2004**, *9*, 3.
- [22] R. Cheng, Y. Shang, D. Hayes Jr., S. P. Saha, G. Yu, *Neuroimage* **2012**, *62*, 1445.
- [23] A. Vermeij, A. S. Meel-van den Abeelen, R. P. Kessels, A. H. van Beek, J. A. Claassen, *Neuroimage* **2014**, *85*, 608.
- [24] L. Bu, J. Li, F. Li, H. Liu, Z. Li, *BMJ Open* **2016**, *6*, e013357.
- [25] R. Cui, M. Zhang, Z. Li, Q. Xin, L. Lu, W. Zhou, Q. Han, Y. Gao, *Microvasc. Res.* **2014**, *93*, 14.
- [26] Q. Tan, M. Zhang, Y. Wang, M. Zhang, B. Wang, Q. Xin, Z. Li, *Microvasc. Res.* **2016**, *103*, 19.
- [27] G. Xu, M. Zhang, Y. Wang, Z. Liu, C. Huo, Z. Li, M. Huo, *PLoS One* **2017**, *12*, e0188329.
- [28] P. Kvandal, S. A. Landsverk, A. Bernjak, A. Stefanovska, H. D. Kvernmo, K. A. Kirkeboen, *Microvasc. Res.* **2006**, *72*, 120.
- [29] Z. Li, M. Zhang, Q. Xin, S. Luo, W. Zhou, R. Cui, L. Lu, *Microvasc. Res.* **2013**, *88*, 32.
- [30] B. L. Edlow, M. N. Kim, T. Durduran, C. Zhou, M. E. Putt, A. G. Yodh, J. H. Greenberg, J. A. Detre, *Physiol. Meas.* **2010**, *31*, 477.
- [31] M. Marinoni, A. Ginanneschi, P. Forleo, L. Amaducci, *Ultrasound Med. Biol.* **1997**, *23*, 1275.
- [32] H. Obrig, M. Neufang, R. Wenzel, M. Kohl, J. Steinbrink, K. Einhaupl, A. Villringer, *Neuroimage* **2000**, *12*, 623.
- [33] C. G. Riberholt, N. D. Olesen, M. Thing, C. B. Juhl, J. Mehlsen, T. H. Petersen, *PLoS One* **2016**, *11*, e0154831.
- [34] M. H. Oudegeest-Sander, A. H. van Beek, K. Abbink, M. G. Olde Rikkert, M. T. Hopman, J. A. Claassen, *Exp. Physiol.* **2014**, *99*, 586.
- [35] A. H. van Beek, J. Lagro, M. G. Olde-Rikkert, R. Zhang, J. A. Claassen, *Neurobiol. Aging* **2012**, *33*, e421.
- [36] M. Reinhard, E. Wehrle-Wieland, D. Grabiak, M. Roth, B. Guschlbauer, J. Timmer, C. Weiller, A. Hetzel, *J. Neurol. Sci.* **2006**, *250*, 103.
- [37] J. A. Claassen, B. D. Levine, R. Zhang, *J. Appl. Physiol.* **2009**, *106*(1), 153.
- [38] H. W. Schytz, A. Hansson, D. Phillip, J. Selb, D. A. Boas, H. K. Iversen, M. Ashina, *J. Stroke Cerebrovasc. Dis.* **2010**, *19*, 465.
- [39] D. Phillip, H. W. Schytz, H. K. Iversen, J. Selb, D. A. Boas, M. Ashina, "Spontaneous Low Frequency Oscillations in Acute Ischemic Stroke – A NearInfrared Spectroscopy (NIRS) Study" *J Neurol Neurophysiol* **2014**, *5*, 1.
- [40] P. Novak, *Neurosci. J.* **2016**, *2016*, 6127340.
- [41] R. Raddino, G. Zanini, D. Robba, I. Bonadei, F. Chieppa, C. Pedrinazzi, G. Caretta, A. Madureri, E. Vizzardi, L. Dei Cas, *Heart Int.* **2006**, *2*, 171.
- [42] B. J. Carey, R. B. Panerai, J. F. Potter, *Stroke* **2003**, *34*, 1871.
- [43] C. van Campen, F. W. A. Verheugt, F. C. Visser, *Clin. Neurophysiol. Pract.* **2018**, *3*, 91.
- [44] R. Cheng, Y. Shang, S. Wang, J. M. Evans, A. Rayapati, D. C. Randall, G. Yu, *J. Biomed. Opt.* **2014**, *19*, 17001.
- [45] R. Zhang, J. H. Zuckerman, B. D. Levine, *J. Appl. Physiol.* **1985**, *85*(1998), 1113.
- [46] R. B. D'Agostino, P. A. Wolf, A. J. Belanger, W. B. Kannel, *Stroke* **1994**, *25*, 40.
- [47] A. A. Bahrani, D. K. Powell, G. Yu, E. S. Johnson, G. A. Jicha, C. D. Smith, *J. Stroke Cerebrovasc. Dis.* **2017**, *26*, 779.
- [48] Y. L. Lian He, Y. Shang, B. J. Shelton, Y. Guoqiang, *J. Biomed. Opt.* **2013**, *18*, 037001.
- [49] W. B. Baker, A. B. Parthasarathy, D. R. Busch, R. C. Mesquita, J. H. Greenberg, A. G. Yodh, *Biomed. Opt. Express* **2014**, *5*, 4053.
- [50] F. Scholkmann, M. Wolf, *J. Biomed. Opt.* **2013**, *18*, 105004.
- [51] M. A. Kamran, M. M. N. Mannann, M. Y. Jeong, *Front. Neuroinform.* **2018**, *12*, 37.
- [52] D. Irwin, L. Dong, Y. Shang, R. Cheng, M. Kudrimoti, S. D. Stevens, G. Yu, *Biomed. Opt. Express* **2011**, *2*, 1969.
- [53] C. Huang, Y. Gu, J. Chen, A. A. Bahrani, E. G. Abu Jawdeh, H. S. Bada, K. Saatman, G. Yu, L. Chen, *IEEE J. Sel. Top. Quantum Electron.* **2019**, *25*, 1.
- [54] C. Haddix, A.A. Bahrani, A. Kawala-Janik, W.G. Besio, G. Yu, S. Sunderam, presented at 22nd Int Conf on Methods and

- Models in Automation and Robotics (MMAR), IEEE, Miedzyszdroje, Poland, August 2017, pp. 642–645.
- [55] A. Farina, A. Torricelli, I. Bargigia, L. Spinelli, R. Cubeddu, F. Foschum, M. Jager, E. Simon, O. Fugger, A. Kienle, F. Martelli, P. Di Ninni, G. Zaccanti, D. Milej, P. Sawosz, M. Kacprzak, A. Liebert, A. Pifferi, *Biomed. Opt. Express* **2015**, *6*, 2609.
- [56] G. Rosenthal, R. O. Sanchez-Mejia, N. Phan, J. C. Hemphill 3rd, C. Martin, G. T. Manley, *J. Neurosurg.* **2011**, *114*, 62.
- [57] H. S. Mangat, *Continuum (Minneapolis Minn)* **2012**, *18*, 532.
- [58] R. W. Regenhardt, A. S. Das, C. J. Stapleton, R. V. Chandra, J. D. Rabinov, A. B. Patel, J. A. Hirsch, T. M. Leslie-Mazwi, *Front. Neurol.* **2017**, *8*, 317.
- [59] J. P. Saul, R. D. Berger, M. H. Chen, R. J. Cohen, *Am. J. Physiol.* **1989**, *256*, H153.
- [60] N. H. Holstein-Rathlou, A. J. Wagner, D. J. Marsh, *Am. J. Physiol.* **1991**, *260*, F53.
- [61] D. Phillip, H. W. Schyetz, J. Selb, S. Payne, H. K. Iversen, L. T. Skovgaard, D. A. Boas, M. Ashina, *Eur. J. Clin. Invest.* **2012**, *42*, 1180.
- [62] D. G. Buerk, C. E. Riva, *Microvasc. Res.* **1998**, *55*, 103.
- [63] H. D. Kvernmo, A. Stefanovska, K. A. Kirkeboen, K. Kvernebo, *Microvasc. Res.* **1999**, *57*, 298.
- [64] A. Mahdi, D. Nikolic, A. A. Birch, S. J. Payne, *Physiol. Meas.* **2017**, *38*, 1396.
- [65] M. A. Mintun, B. N. Lundstrom, A. Z. Snyder, A. G. Vlassenko, G. L. Shulman, M. E. Raichle, *Proc. Natl. Acad. Sci. U. S. A.* **2001**, *98*, 6859.
- [66] T. Hayashi, H. Watabe, N. Kudomi, K. M. Kim, J. Enmi, K. Hayashida, H. Iida, *J. Cereb. Blood Flow Metab.* **2003**, *23*, 1314.
- [67] H. S. Markus, *J. Neurol. Neurosurg. Psychiatry* **2004**, *75*, 353.
- [68] C. Gregori-Pla, I. Blanco, P. Camps-Renom, P. Zirak, I. Serra, G. Cotta, F. Maruccia, L. Prats-Sanchez, A. Martinez-Domeno, D. R. Busch, G. Giacalone, J. Marti-Fabregas, T. Durduran, R. Delgado-Mederos, *J. Neurol.* **2019**, *266*, 990.
- [69] A. H. Van Beek, J. A. Claassen, *Behav. Brain Res.* **2011**, *221*, 537.
- [70] J. H. Z. Rong Zhang, B. D. Levine, *J. Appl. Physiol.* **1998**, *85*, 1113.
- [71] N. R. Cook, N. P. Paynter, C. B. Eaton, J. E. Manson, L. W. Martin, J. G. Robinson, J. E. Rossouw, S. Wassertheil-Smoller, P. M. Ridker, *Circulation* **2012**, *125*, S1741.
- [72] T. Li, Y. Lin, Y. Shang, L. He, C. Huang, M. Szabunio, G. Yu, *Sci. Rep.* **2013**, *3*, 1358.
- [73] Y. Shang, R. Cheng, L. Dong, S. J. Ryan, S. P. Saha, G. Yu, *Phys. Med. Biol.* **2011**, *56*, 3015.
- [74] L. Gagnon, M. A. Yucel, M. Dehaes, R. J. Cooper, K. L. Perdue, J. Selb, T. J. Huppert, R. D. Hoge, D. A. Boas, *Neuroimage* **2012**, *59*, 3933.
- [75] Y. Zhang, X. Liu, Q. Wang, D. Liu, C. Yang, J. Sun, *Comput. Assist. Surg.* **2019**, *24*, 144.
- [76] T. J. Farrell, M. S. Patterson, M. Essenpreis, *Appl. Optics* **1998**, *37*, 1958.
- [77] X. Zhang, Z. Gui, Z. Qiao, Y. Liu, Y. Shang, *Biomed. Opt. Express* **2018**, *9*, 2365.
- [78] Y. Shang, G. Yu, *Appl. Phys. Lett.* **2014**, *105*, 133702.
- [79] Y. Shang, T. Li, L. Chen, Y. Lin, M. Toborek, G. Yu, *Appl. Phys. Lett.* **2014**, *104*, 193703.
- [80] Z. Li, M. Zhang, Q. Xin, S. Luo, R. Cui, W. Zhou, L. Lu, *J. Cereb. Blood Flow Metab.* **2013**, *33*, 692.
- [81] J. Li, C. S. Poon, J. Kress, D. J. Rohrbach, U. Sunar, *J. Biophotonics* **2018**, *11*, e201700165.
- [82] D. Wang, A. B. Parthasarathy, W. B. Baker, K. Gannon, V. Kavuri, T. Ko, S. Schenkel, Z. Li, Z. Li, M. T. Mullen, J. A. Detre, A. G. Yodh, *Biomed. Opt. Express* **2016**, *7*, 776.

How to cite this article: Bahrani AA, Kong W, Shang Y, et al. Diffuse optical assessment of cerebral-autoregulation in older adults stratified by cerebrovascular risk. *J. Biophotonics*. 2020;13: e202000073. <https://doi.org/10.1002/jbio.202000073>